Hindawi
Geofluids
Volume 2023, Article ID 2184880, 15 pages
https://doi.org/10.1155/2023/2184880

Research Article

Damage Depth Test and Numerical Simulation of Stope Floor in Mining Face

Xipeng Cui,[1,2] **Hongqi Shao**,[3] **and Kailei Zhao**[2]

[1]*School of Architecture and Civil Engineering, Xi'an University of Science and Technology, Xi'an, Shaanxi 710054, China*
[2]*China Coal Xi'an Design Engineering Co., Ltd., Xi'an, Shaanxi 710054, China*
[3]*Xi'an Research Institute of China Coal Technology & Engineering Group Corp., Xi'an, Shaanxi 710077, China*

Correspondence should be addressed to Xipeng Cui; 360209084@qq.com

Received 11 March 2023; Revised 18 July 2023; Accepted 17 August 2023; Published 13 September 2023

Academic Editor: Qiqing Wang

The purpose of this study is to explore the development depth of rock layer rupture and analyze the developmental regularity of mining floor in Dongsi mining area of Xinzhi Coal Mine. Two kinds of pressure water testing methods and numerical simulation are used to study the failure characteristics of the bottom plate of the working face in Dongsi mining area of Xinxian Coal Mine. The results show that the failure of working face bottom plate starts from a certain range in front of the working face. With the advance of working face, the failure depth of mining bottom plate increases continuously. At the same time, the failure range of mining roadway is slightly larger than the failure range of working face bottom plate due to the double disturbance of tunneling and mining. The pressure water test shows that the rupture depth occurs at 8.98-9.03 m. The numerical simulation results of floor failure depth show that its depth is about 8.7 m, which is basically consistent with the pressure water test. It provides a reference for the advanced preexploration of mining bottom plate failure in similar coal seam.

1. Introduction

At present, belt pressure mining is the main mining method for coal mining in confined aquifer. However, to realize belt pressure mining, it is necessary to fully understand and grasp the degree of mining deformation and damage of bottom plate and the water-resisting ability of mining bottom plate. The theory and practice show whether safety belt pressure mining can be realized and the belt pressure size and the degree and characteristics of deformation and damage of the bottom plate are of great significance to the water barrier ability of the bottom plate. Therefore, the analysis and evaluation of deformation and failure law of floor mining is the key theory and application technology of water hazard prevention and control in coal mine floor.

Water inrush from floor is a typical "mining effect," that is, the stress and strain phenomenon of coal floor under the action of mining pressure. Before coal seam mining, the floor rock mass is in the original stress balance state. After mining, the goaf provides free space for the movement of rock mass, prompting the deformation of floor rock mass, thus causing the damage of original balance state, forming additional stress, resulting in the deformation and damage of floor. Compared with roof, the research on the deformation and failure law of floor is relatively late, which is mainly due to the development of mining to the deep part in the late 1970s, and the sudden water is becoming more and more serious; people only recognize the importance of studying the movement law of floor; the previous work neglected the unity of deformation of roof and floor and lacked the understanding of the internal law of rock mass movement of floor; the field observation data of floor are scattered, difficult, and expensive, thus making the research work on rock water of coal mine floor slowly progressing and having little effect. Before the study, the former Soviet Union Stresslev firstly conducted theoretical analysis on the rock mass of coal seam floor in 1948, [1] simplified the coal seam floor into two ends of fixed support, subjected to uniform load, analyzed its deformation and failure, and established the prediction theoretical formula of floor protrusion. Jincai et al. [2] proposed the concept of "lower three zones" for seam failure in coal seam goaf floor in 1981, namely, bulging

crack zone (8-15 m), small deformation and movement zone (20-25 m), and stress microchange zone (60-80 m).

After coal seam mining, the original stress balance state of floor rock layer is damaged, the stress concentration is generated around the goaf, and each point of floor rock layer undergoes the process of "supporting pressure concentration compression-stress relief expansion-stress recovery and recompression". It is these stresses that make the fracture rate of floor rock layer change, and three kinds of fractures, vertical tension fracture, layer-to-layer fracture, and shear fracture, are generated in floor rock layer, thus making this part of floor rock layer lose the water barrier ability. The depth of floor failure refers to the mining process of working face recovery. Due to the comprehensive action of mineral pressure and other factors, the coal seam floor produces a certain depth of damage and the rock layer with water conductivity. At present, many experts and scholars have conducted research on the accurate determination of the damage depth of coal seam floor caused by mining.

Based on the theory of "three bands," Longqing and Jin [3] proposed the division of "four bands" for the bottom plate of mining coal seam; Fangjun et al. [4] used I-steel girder to control and monitor the pressure of the bottom plate of coal seam; Hao and Quan [5] established the calculation model of the limit balance depth of roadway bottom plate by means of field measurement, similarity simulation, and numerical simulation and concluded that the width of the limit balance area of roadway is linearly increasing with the depth of roadway bottom plate failure; Zhang Jiachen [6] analyzed the failure characteristics of the bottom plate of coal seam by gradually modifying the model boundary conditions, repeatedly adjusting the mechanical parameters, etc., combined with the results of field measurement, and revealed the propagation law of mineral pressure in the bottom plate; Jiachen et al. [7], based on the saddle failure law of the bottom plate and the test principle of direct current method, studied the changes of the electrical characteristics of the bottom plate rock layer in the recovery process of working face; Haifeng and Duoxi [8] regarded the bottom plate-layered rock mass as a transverse isotropic continuum and deduced the load distribution characteristics of coal seam, based on the nonlinear analysis of mining depth. A deep coal seam bottom plate failure depth model was constructed, and a new prediction formula for the bottom plate failure depth was fitted; similar simulation experiments were conducted for the bottom plate of confined water by Yaodong et al. [9], Yixin et al. [10], Gao Shang [11], and Niu Xiuqing [12] to study the bottom plate failure depth; Cheng et al. [13] and Pingsong et al. [14] used CT technology to obtain the dynamic development rule and deformation failure characteristics of the bottom plate failure during coal seam mining. Fan, Kaifang et al. [15], Yang, Zhongping et al. [16] describe the evolution process of rock separation and instability from the aspects of dynamic evolution and spatiotemporal evolution, respectively. Li et al. [17] analyzed the underground pressure behavior during mining and verified the effectiveness of floor grouting reinforcement control technology through microseismic monitoring.

With the development of modern geophysical exploration technology, most of the seismic monitoring methods such as microseismic monitoring technology, borehole observation, or optical fiber testing are used to measure and analyze the floor disturbance depth, but the microseismic error is large, the precision is low, and there is no unified criterion. Due to the factors such as water quality and gas in the hole, the microscopic cracks cannot be distinguished in detail, and it is difficult to give a qualitative conclusion. Optical fiber testing also faces problems such as the coupling between the sensor cable and the borehole surrounding rock which is difficult to control, the physical properties of the original rock are destroyed by grouting sealing, and the installation process of the optical fiber cable is complicated, which still needs to be further improved and developed.

Therefore, two kinds of embolization dynamic sectional water pressure test technology methods are adopted this time, which will not have any influence on the production of the working face, and the measurement accuracy is high, the test results are accurate, and the data is intuitive and easy to distinguish.

In the past, scholars used different methods to study the deformation and failure law of coal seam floor from different angles and achieved a lot of results. However, the hydrogeological conditions of the working face are more complicated, and the research on the failure law of floor mining under confined water condition is relatively few. Therefore, according to the special geological conditions of 10-409 working face in Xindi Coal Mine, two kinds of plugging water injection methods are adopted to analyze and determine the mining failure depth of the working face floor, and then, the failure depth value obtained by numerical simulation analysis is mutually verified, which provides an important theoretical basis for safe mining in this area.

2. Engineering Overview

The coal mine is located at the southernmost end of Huozhou City, Shanxi Province, People's Republic of China, in the middle of Huoxi Coal Field (Figure 1). Its administrative division is located in Huozhou City and Xinfen City, and its geographical location is located at the northern edge of Linfen City, Shanxi Province, covering part of Xinhui Town, Taotangyu Township, Zhao Town, and Xingtang Temple Township. The north of the field is adjacent to Caozhuang Mine, the boundary faults are from south to south, the west is bounded by riverbed faults and Chiyu faults, and the east is 11# coal seam bedrock outcrop line, with a mine area of 77.48 km^2 and a design capacity of 2.5 million tons/year. Currently there are 2#, 10#, and 11# coal seams mined, with two production levels (+540 m and +450 m) and two production mining areas (Dongsi mining area and left wing mining area).

Dongsi mining area exploits Taiyuan Group 10# coal seam and subsequently exploits 11# coal seam. The two coal seams are located between Taiyuan Group K_2 limestone and Ordovician limestone aquifer, the distance between 10# coal seam and 11# coal seam is about 10 m, and the distance between 11# coal seam and Lower Ordovician limestone is

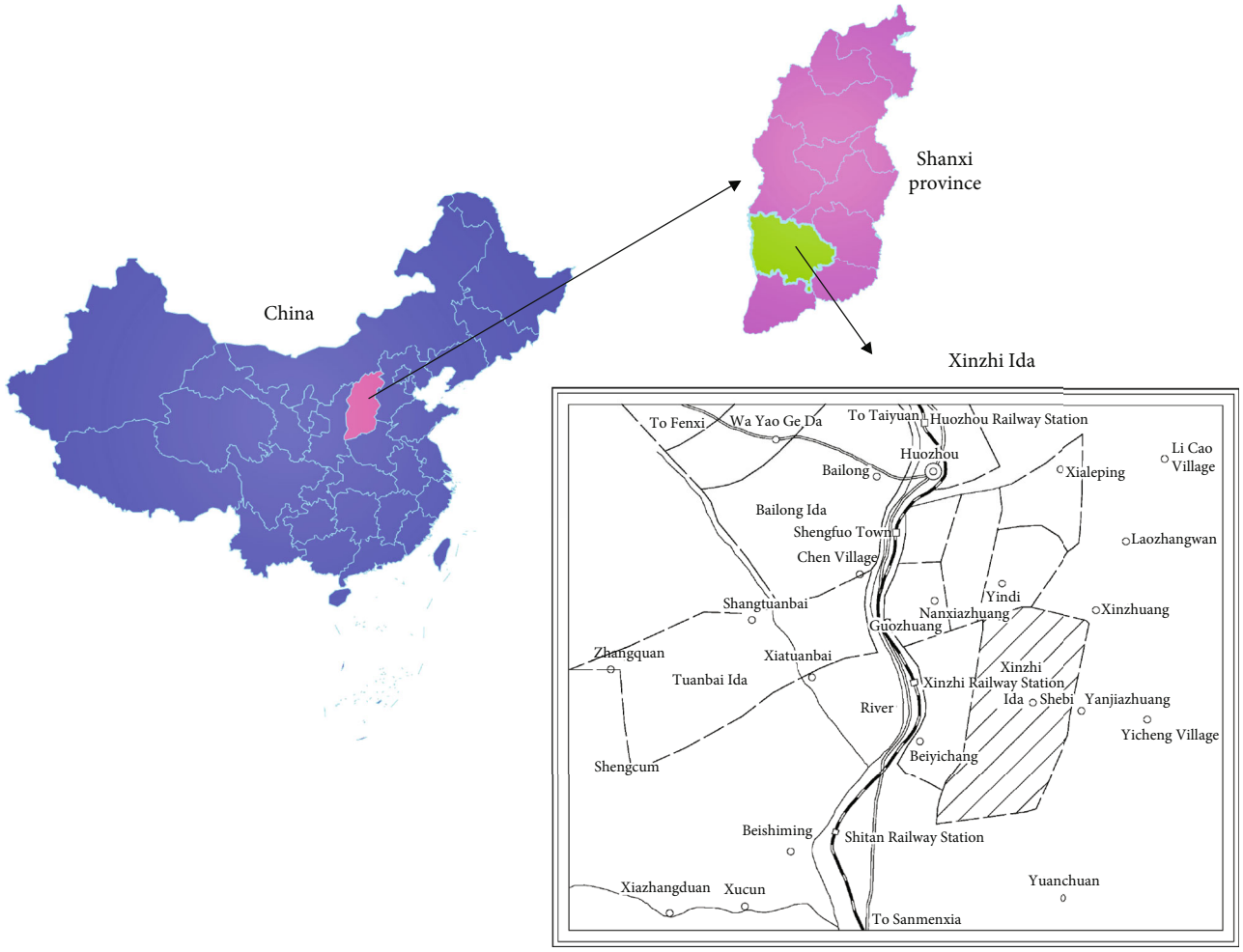

Figure 1: The location map of the study area.

about 20 m. The mining elevation of two coal seams is below the Ordovician limestone water line (about +500 meters), which is compressed mining (Figure 2).

The test face is 10-409 working face, which is located at +540 level in Dongsi mining area, the ground elevation is +723 m~+790 m, the working face elevation is +416 m~+448 m, the working face strike length is 1002 m, and the inclination length is 180 m. The average coal seam thickness is 2.63 m and the dip angle is 6°. The working area is the goaf of 10-407 working face in the north, belt and track roadway in the west, and tunneling roadway of 10-411 working face in the south. At the time of digging, a coal pillar with width of 30 m is set aside between the coalfaces.

The upper loess cover thickness reached 73 m~120 m, and the bedrock thickness was 172 m~187 m. There are three subsidence columns in the working face, which are 175# subsidence column, long axis length 45 m, strike N35°, short axis length 27 m, and subsidence angle 86°; 176#subsidence column, long axis length 30 m, strike N20°, short axis length 20 m, and subsidence angle 85°; and 177# subsidence column, long axis length 35 m, strike N16°, short axis length 20 m, and subsidence angle 85°. There are 5 faults with drop less than 2 m. The working face is directly topped with 9# coal and 1.8 m thick black, thin mudstone. Loading is K_2 limestone, dark gray, dense and hard, and 8.5 m thick. The direct bottom is sandy mudstone with a thickness of 1.5 m, and the old bottom is medium sandstone with a thickness of 5.5 m (Figure 3).

In general, the maximum depth of mining failure of floor rock layer occurs at 3~5 m near the alley inside the working face [18], so the horizontal projection of the test section arranged in this test is at 3~5 m inside the working face. The observation time is arranged according to the excavation schedule.

3. Test Method

The pressurized water test is more mature and has been applied in the monitoring of the rupture depth of the floor in China since the seventies and eighties and has achieved good results.

There are also water conservancy and hydropower "pressurized water test procedures" can refer to, so this choice of pressurized water test methods.

3.1. Field Test Method. Two methods of water pressurization were tested in the field, single embolic water barrier test and double embolic segmented water barrier test.

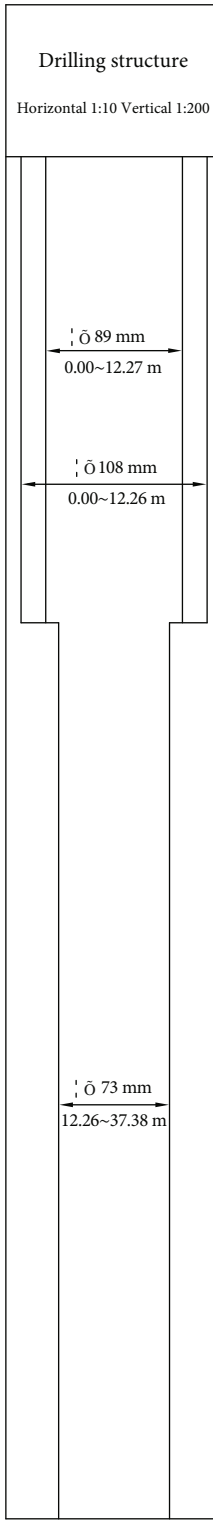

Layer number	Rock formation name	Layer thickness (m)	Cumulative thickness (m)	Lithology description
1	Coal	0.23	0.23	Green six feet.
2	Shale	0.67	0.90	Carbonaceous striped, containing plant fossils.
3	Sandstone	5.20	6.10	Contains quartz, mica, pyrite, fine particles in the upper part, medium particles in the middle part, fine particles in the lower part, carbonaceous stripes, good sphericity and poor sorting performance.
4	Sandy mudstone	4.10	10.20	Dark gray, containing muscovite flakes, pyrite and plant fossils, with well-developed bedding, and more pyrite from the upper part.
5	Coal	1.85	12.05	Up to eight feet.
6	Sandstone	2.50	14.55	Black, fine-grained, quartz sandstone at the top, containing muscovite flakes, dense, with carbonaceous streaks.
7	Shale	1.50	16.05	Black, containing mica, brittle and dense.
8	Limestone	0.20	16.25	Contains calcite veins.
9	Bauxite mudstone	1.75	18.00	Off-white, oolitic structure, containing plant fossils.
10	Sandstone	5.00	23.00	White, quartzy, dense, hard, massive structure.
11	Shale	2.10	25.10	Dark gray with gray top and black bottom.
12	Bauxite mudstone	3.80	28.90	Gray, a little white, oolitic structure.
13	Austrian gray	8.48	37.38	Gray, light gray, gray black, microcrystalline structure, dense, brittle, irregular cracks can be seen locally, filled with calcite veins.

Figure 2: Drilling column diagram of lane 10-4112 in Xindi Coal Mine.

3.1.1. Single Embolic Water Pressurization Test. The single embolic pressurization test is to place the test segment at the bottom of drilling hole, bare hole of test segment, and cannula under nontest segment for pressurization test.

3.1.2. Double Embolic Segmented Water Pressure Test. The double embolic segmented pressurization test is to seal both ends of the test segment and perform the pressurization test on the test segment.

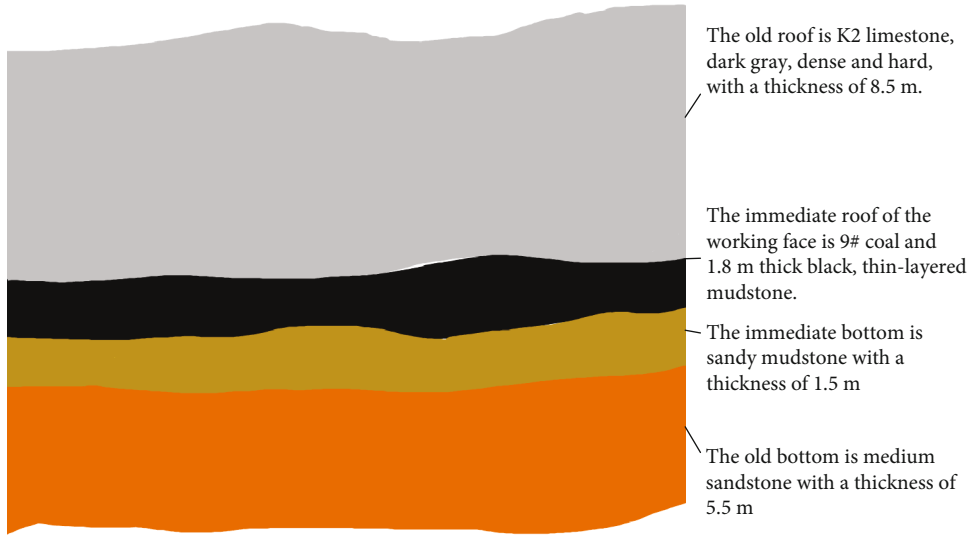

Figure 3: The regional structural map.

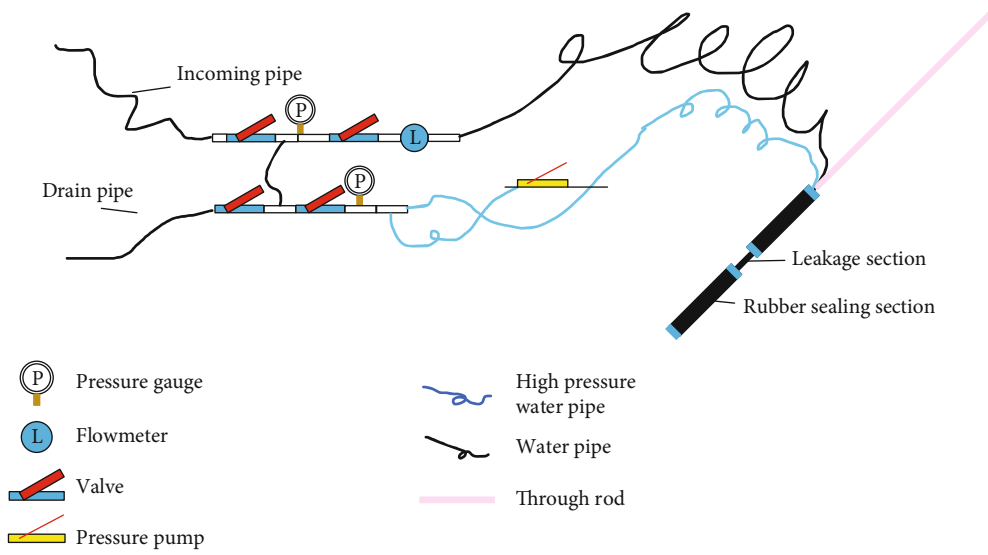

Figure 4: Schematic diagram of pressurized water device.

The rock layer on the floor is ruptured under the mining pressure, and the length of the test section is about 2 m. The pressure of the water pressure test is P=0.2 MPa, and the water pressure time is 15 min~25 min. The observation is recorded every 5 min, and 4~5 sets of data are read for each test.

The device adopts the autocratic GY drilling pressure water test device of Xi'an Research Institute Co., Ltd., China Coal Science and Industry Group, as shown in Figure 1. The principle of this device is to use special water sealing equipment to isolate a certain length of drilling test section and then use a fixed water head to drill water into this section, according to the calculation of rock water absorption to understand the development of rock cracks and water permeability in situ test device (Figure 4).

3.2. Test Procedures

(1) Connect the test instrument well: according to the schematic diagram in Figure 4, connect the test instrument well. It is noted that the measuring range of pressure gauge 1 is 2~4 times of inlet water pressure, and the measuring range of pressure gauge 2 is 2~4 times of designed pressure

(2) Engage the pass-through rod and insert the water stop plug into the test segment; note that during the connection, screw connection is used between the pass-through rod and pass-through rod as well as between the pass-through rod and water stop plug. In the connection and test, reverse rotation

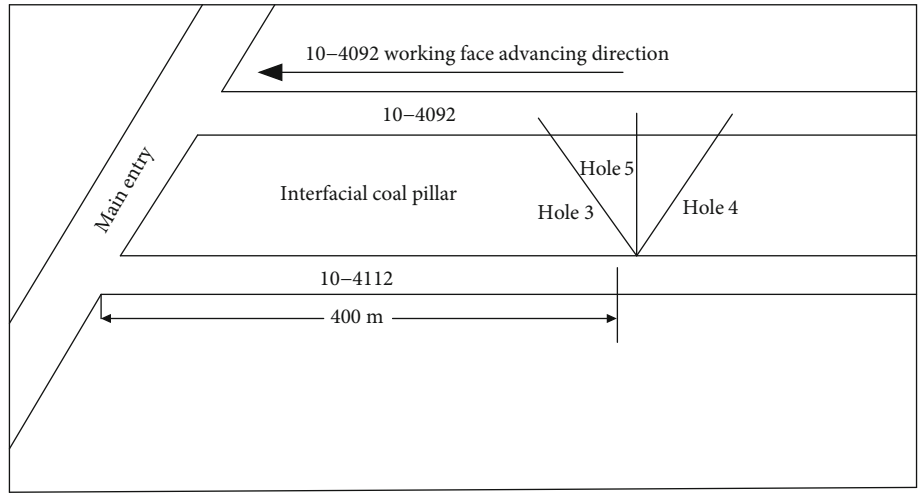

Figure 5: Layout of drilling rigs for pressure water test.

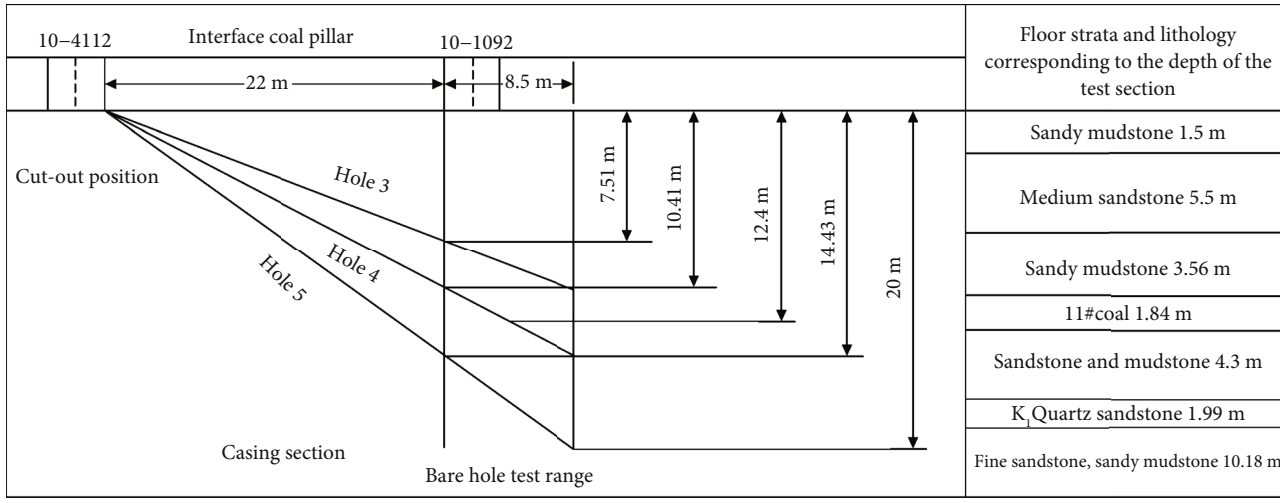

Figure 6: Schematic diagram of drilling hole layout.

should be avoided as far as possible; otherwise, it may cause the water stop plug to drop. Close all valves ready to start test

(3) Stopper pressurization: after the stopper is confirmed to enter the predetermined test segment position, the stopper starts pressurization. Pressurization process: open valves 1 and 4, water stop plug starts to pressurize, when the pressure of pressure gauge 3 is 1.5~2 MPa, pressure ends, and close valve 4. If the pressure of water stop plug is less than 1.5 MPa, add water into the pressure pump to pressurize the water stop plug

(4) Pressurized water observation: when the stopper is closed, pressurized water is started. Open valve 2, observe pressure gauge 2, confirm if the reading of pressure gauge is basically stable at the designed pressure, and start the test; the test process generally takes 15~25 min. Record the flow rate of flow meter every 5 minutes, and observe for 4~5 times. If the pressurized water volume changes greatly every other interval, exceeding 10%, observe more than one group. At the end of observation and recording, inspect the records to ensure the accuracy and legibility of records

3.3. Test Process

3.3.1. Drill. Drilling holes are arranged in 10-4112 roadway, and a total of 3 boreholes are constructed, shown in Figure 5.

Size of drilling hole: the dig is located in lane 10-4112, shown in Figure 6. Drilling in the field lasted 54 days, drilling 191.64 m. Drilling equipment: select Hangzhou Drill Type IIIA Drill, KBY double fluid grouting pump, and its corresponding supporting equipment.

Drill combination: use 50 inner wire drill pipe, add anti-oblique centralizer, and maintain sufficient drilling pressure.

Table 1: List of drilling parameters.

Bit type	Specifications (mm)	Pressure (kN)	Water volume (m^3/h)	Revolutions (r/min)
Coreless bit	ϕ108	8-20	5-10	48-100
	ϕ73	30-60	5-10	48-100

Table 2: Statistical table of borehole construction data.

Project	Dip angle (°)	Hole depth (m)	Opening diameter ϕ (mm)	Casing length (m)	Final hole diameter ϕ (mm)	Bare hole
3# hole	-19	38.02	108	24.10	73	24.10 m-38.02 m
4# hole	-25	38.62	108	29.90	73	29.9 m-38.62 m
5# hole	-33	38.62	108	26.4	73	26.4 m-38.62 m

Table 3: Permeability coefficient of each test section.

Test depth	K_1	K_2	K_2/K_1	ΔK
7.51~12.37 m	13.87	16.43	1.184092	2.554655
8.98~9.03 m	2.112	50.36	23.83333	48.224
9.96~10 m	282.74	320.32	1.132898	37.576
10.94~11 m	97.5	109.64	1.124549	12.144
12.4~14.43 m	0.069	0.192	2.753813	0.1218578

Note: 7.51~12.37 m is 3# pore single embolic pressurization test result; 8.98~9.03 m, 9.96~10 m, and 10.94~11 m are 3# pore double embolic pressurization test result; and 12.4~14.43 m is 4# pore single embolic pressurization test result.

Different drill bits of different specifications are combined with different drill tools.

Drilling method: 3, 4, and 5 drilling with rock core drill bit were used.

Flushing fluid: use full-hole clear water to drill.

Drilling parameters: in drilling, master the improved number, pressure, water supply, and other technical parameters (Table 1) and (Table 2).

3.3.2. Test. The field test lasted 65 days. Three observations were conducted in hole 1#, two in hole 2#, and 64 in the bottom plate rupture depth. Nearly 200 sets of data were obtained.

3.4. Outcome Analysis

3.4.1. Determination of Mining Damage Depth. After the pressure water test, the rock permeability coefficient at the pressure water position is determined according to the following formula:

$$K = \alpha \frac{Q}{LP}, \tag{1}$$

where K is the permeability coefficient (m/d), Q is the steady flow rate during pressure water test (m^3/d), P is the pressure applied during pressure water test segment (MPa), L is the length of water pressure section (m), and α is the coefficient (range 1~1.2).

The change of the permeability coefficient of the floor of the working face before mining and after mining reflects the degree of damage to the floor of the mining face. The increment of postmining and premining permeability coefficients $\Delta K \geq 0.2$ (m/d) and the ratio of postmining and premining permeability coefficients $K_2/K_1 \geq 2$ are used as the discriminant index of floor failure depth.

When the hole is fully pressurized, the length of hole 3# is 13.92 m, and the length of test segment of hole 4# is 8.72 m. In the calculation, 1.1 is taken to obtain Table 3.

According to the criterion, the rupture depth occurred at 8.98~9.03 m.

3.4.2. Test and Rupture Process Analysis. In this test, the impaction fracture depth is determined by injecting water through embolism method, the working face is advanced from east to west, the test sections are arranged as 4# hole, 5# hole, and 3# hole from east to west according to hole number, and the test depth is closed as 12.4~14.43 m, 14.43~20 m, and 7.51~12.37 m. The test was started approximately 40 m from the working face to hole 4#. The test results are shown in Figures 7–10.

The following is the description of the test process: the starting position for test is 4# bore working face 40 m. During the measuring process, it can be seen that the water pressure per unit time of hole 4# is very small, the test results of hole 5# are basically unchanged except for a certain effect in the initial development, and it is preliminarily determined that the rupture depth is less than the test depth of hole 5#, so the accuracy of the test of holes 3# and 4# is strengthened, and the water pressure test of hole 5# is stopped. During the test, the background value of single embolization and double embolization water pressure is tested for each test hole. In the daily test, single embolic test is generally

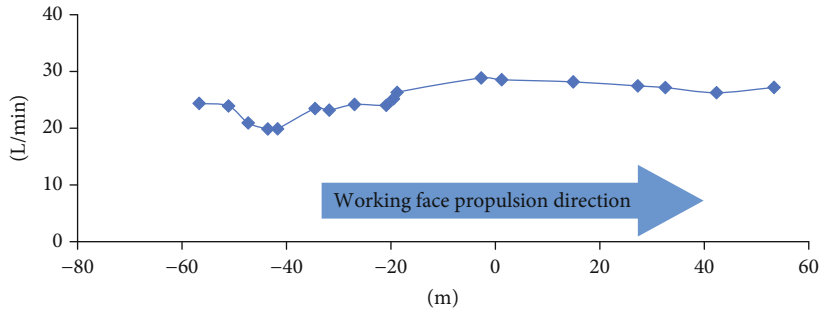

Figure 7: Pore pressure water volume variation diagram (7.51~12.37 m).

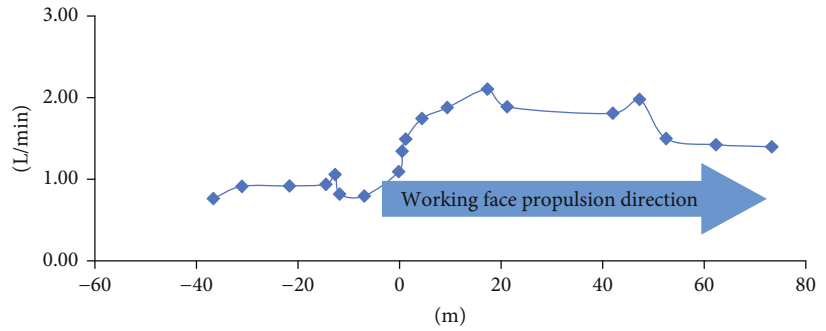

Figure 8: Pore water volume variation diagram (12.4-14.43 m).

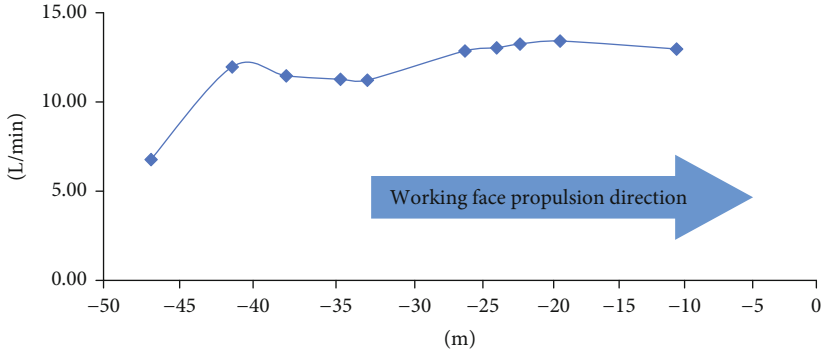

Figure 9: Pore water volume variation diagram of 5# (14.43 m~20 m).

adopted. If the test result varies greatly from the previous test result, double embolic test is adopted to accurately determine the changed result.

(A) Curve analysis of total pore water volume change of each hole

3# hole pore pressure water volume changed greatly, the maximum and minimum pressure water volume were 28.6 L/min and 19.8 L/min, respectively, and the pressure water volume curve changes complicatedly, indicating that the permeability coefficient of the test segment of hole 3# changed differently, and the change mode of different segments was also different, which can be seen in the test diagram of hole 3#; for example, in the -45 m~-20 m interval, the pressure water volume of the test segment of hole 8.98 m~9.03 m showed an increasing trend, the pressure water volume of the test segment of hole 9.96 m~10 m showed a decreasing trend, and the pressure water volume of the test segment of hole 10.94 m~11 m was basically unchanged. Looking at the total amount of pressure water in hole 4#, the maximum pressure water volume and the minimum pressure water volume are 2.11 L/min~0.76 L/min, respectively, with little change, but from the trend point of view, there is basically no change from -40 m to 0 m, it starts to increase from 0 m, and it basically remains unchanged from 20 m. The amount of pore water at 5# remains essentially unchanged. It can be seen that the rock bed mining rupture occurred in the 3# hole test section. Well 4# has some impact, but the impact is not significant. Well 5# has essentially no effect.

(B) Detailed analysis on the change of each pore pressure water volume curve

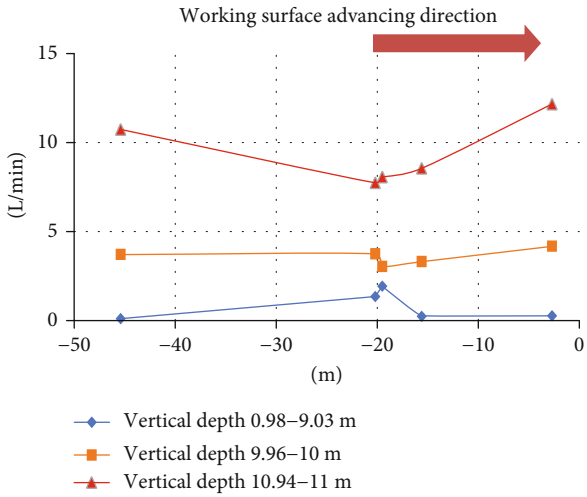

Figure 10: Water pressure variation diagram of 3# pore double stopper.

(1) Analysis on the process of water pressure of hole 3# (full hole) advancing with the cutting eye of working face (Figure 7)

In 3# hole test depth from 7.51 m to 12.37 m, when the working face eye is advanced to the horizontal distance about -50 m from the test point, the water pressure starts to change and gradually decreases; from -40 m to -20 m, the water pressure starts to recover and basically remains unchanged; from -20 m, it starts to gradually increase; from -20 m to 0 m, it reaches the maximum and then basically remains unchanged. In general, the influence of mining on the pore pressure water volume of 3# starts from -50 m and from -50 m to -40 m; it is a process of gradually increasing stress. In this process, the maximum principal stress gradually increases, but the rock mass has not ruptured, which belongs to the compaction stage of rock mass compression process. At this time, the fracture gradually closes and the pressurized water volume gradually decreases. From -40 m to -20 m, the crack in rock mass develops to a certain extent. At this time, with the increase of maximum principal stress, it belongs to the elastic stage of rock mass compression process. At this time, the crack size of rock mass is basically unchanged, so the pressure water volume is basically unchanged. The process from -20 m to 0 m belongs to the plastic deformation stage of rock mass under pressure. At this time, the rupture becomes larger, and the water pressure becomes larger. At 0 m, the maximum principal stress started to decrease, the horizontal stress perpendicular to the advance direction of the working face started to increase, the horizontal crack started to squeeze, the horizontal crack started to decrease gradually, and the water pressure started to decrease slowly.

(2) Analysis of the process of water pressure of hole 3# (segmented) advancing with the cutting eye of working face (Figure 10)

During the test, the double stopper is the test method used when the single stopper changes greatly, so as to accurately determine a layer with the maximum change when the total pore pressure water volume changes greatly. So the double plug test is mainly distributed before 0 m of hole 3#. According to formula (1), it can be concluded that only the ratio of the difference between the maximum pressure water volume and the minimum pressure water volume of 8.98 m~9.03 m meets the criterion in the segmented test results in hole 3#, so only this segment ruptures. Because the ratio of the maximum to the minimum water pressure of the test section with the depth of 9.96 m~10 m does not meet the criterion, the fracture of the test section does not occur completely. Buried in 10.94 m~11 m test segment test results, the basic distribution of water pressure around 4 L/min, the results and 4# hole results are similar, the entire change of water pressure is small, and there is no rupture. It can be seen that the floor rock layer rupture has not yet developed to this depth. This paper analyzes the test results of 3# perforated double stopper: firstly, the change of pressure water volume from -45 m to -20 m is observed. In this interval, the pressure water volume of the test section with vertical depth of 8.98 m~9.03 m gradually increases, the pressure water volume of the test section with vertical depth of 9.96 m~10 m gradually decreases, and the pressure water volume of the test section with vertical depth of 10.94 m~11 m basically remains unchanged.

(i) Stage analysis from -45 m to -20 m: in the process from Figures 11 and 12, the vertical pressure on the bottom plate gradually increases and is in the compaction stage and elastic yield stage. At the same time, vertical shear action will be formed in the stress concentration area. In the places with larger secondary stress, such as the buried depth in the test section of 8.98 m~9.03 m, the rock mass will move towards the mining direction at this time, the fracture will increase, and the water pressure will also increase. Because the secondary stress concentration is not larger than that of 8.98 m~9.03 m and because the upper part moves to the mining region, a deflected curvature will be formed in this region. At this time, the water pressure of the buried test section becomes smaller. Because there is no obvious effect on the stress concentration of the test section with the depth of 10.94 m~11 m, the water pressure is basically unchanged

(ii) -20 m~-15.1 m stage: the water pressure of the test section buried at 9.96 m~10 m and 10.94 m~11 m increases, indicating that at this stage, the rock mass part is plastic damaged, the fracture increases, and the water pressure increases. Buried in 8.98 m~9.03 m test section in this stage, the water pressure gradually decreased, indicating that in this stage, the bottom plate is under the influence of lateral horizontal pressure and vertical stress concentration and the fracture in the ruptured rock mass is compacted; at this time, the water pressure gradually decreased

(iii) -15.1 m~0 m and the stage after 0 m (Figures 13 and 14): in this stage, due to the further concentration

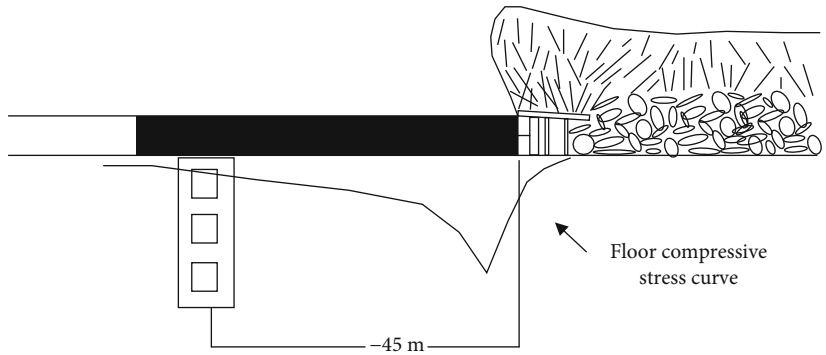

Figure 11: Schematic diagram of the test section at -45 m of the cutting eye.

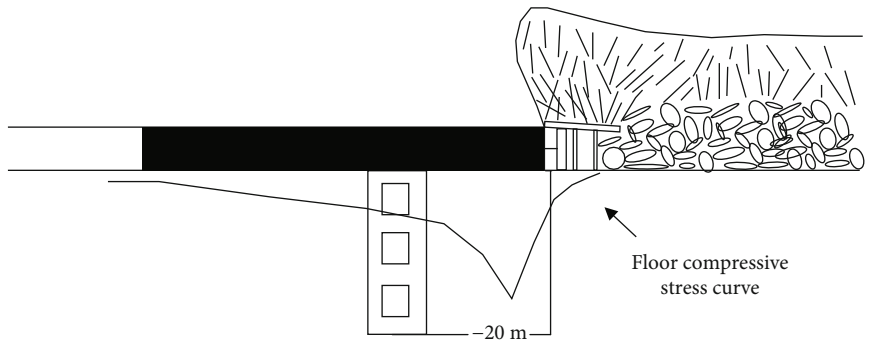

Figure 12: Schematic diagram of the test section at -20 m of the cutting eye.

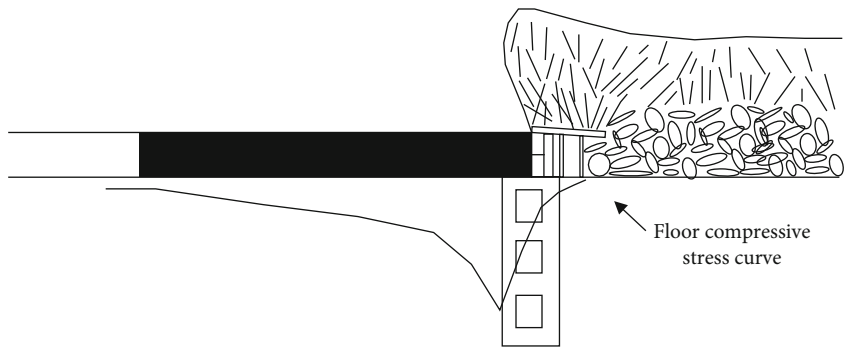

Figure 13: Schematic diagram of the test section at 0 m of the cutting eye.

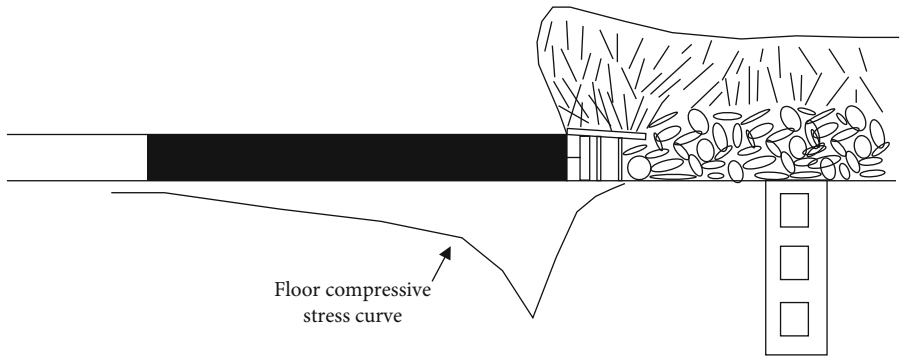

Figure 14: Compression diagram of the test section after the cutting eye.

Table 4: List of rock mass parameters.

	Thickness(m)	Bulk modulus (GPa)	Shear modulus (GPa)	Cohesion (MPa)	Angle of friction (°)	Tensile strength (MPa)
Top plate	120	4.872	3.065	5.56	41	1
Coal seam	2.6	1.952	0.953	1.98	35.1	0.429
Sandstone	5.1	3.533	2.12	4.758	39.09	1.618
Sandy mudstone	4.1	2.235	1.152	1.651	32.47	0.586
Coal seam, bauxite mudstone	9.8	1.952	0.953	1.98	35.1	0.429
Sandstone	5	3.533	2.12	4.758	39.09	1.618
Shale, bauxite mudstone	5.9	1.875	0.865	1.25	39	0.303
Limestone	9.5	5.655	3.893	3.46	36.03	0.48

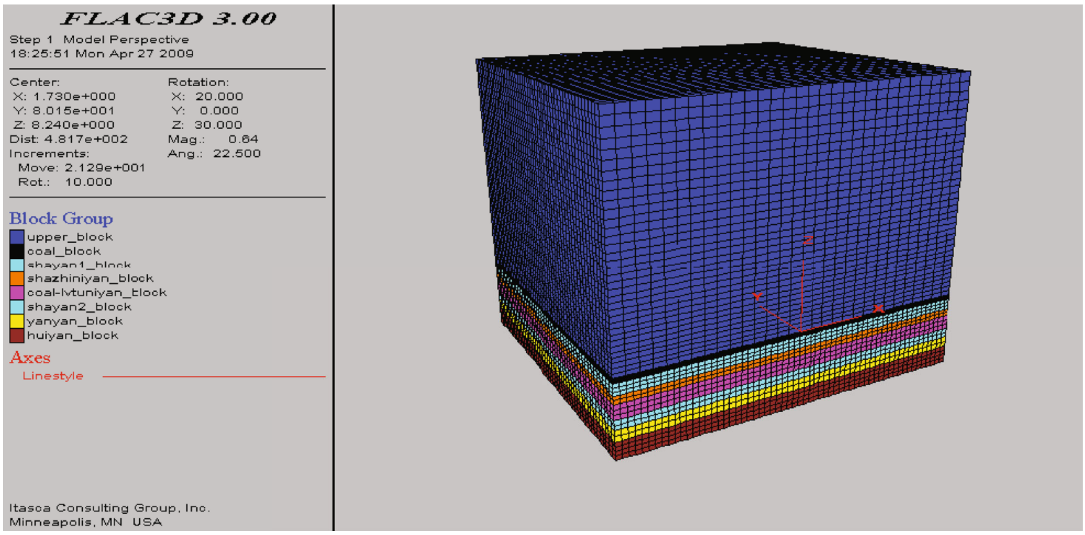

Figure 15: Geological model map.

of vertical stress and the further increase of the difference of lateral pressure, the fracture of floor rock mass gradually increases, and at this time, the water pressure of all buried test segments begins to increase

(3) Analysis of the pore pressure water volume propulsion process of 4# with the cutting eye of working surface (Figure 8)

The fracturing process of pore 4# can be divided into three stages, from -40 m to -15 m, the fracture in rock mass develops to a certain extent, and then, with the increase of maximum principal stress, it belongs to the elastic stage of rock mass compression process. At this time, the fracture size of rock mass is basically unchanged, so the pressurized water volume is basically unchanged. The process from -15 m to 18 m belongs to the plastic deformation stage of rock mass under pressure. At this time, the rupture becomes larger, and the water pressure becomes larger. By 18 m to 80 m, the maximum principal stress reached the maximum and then began to decrease, the horizontal stress perpendicular to the advance direction of the working face began to increase, the horizontal crack began to squeeze, the horizontal crack began to decrease gradually, and the water pressure began to decrease slowly. But in the overall analysis, the water pressure of hole 4# is much less than that of hole 3#, and the maximum water pressure is 2.11 L/min, much less than the maximum water pressure of hole 3# 28.9 L/min;

Table 5: List of basic unit numbers of each rock layer of the model.

Z direction	Actual	Number of units	Density (g/m^3)
Top plate	120	35	2.62
Coal seam	2.6	2	2.55
Sandstone	5.1	3	2.58
Sandy mudstone	4.1	2	2.57
Coal seam, bauxite mudstone	9.8	3	2.55
Sandstone	5	2	2.58
Shale, bauxite mudstone	5.9	2	2.55
Limestone	9.5	4	2.64

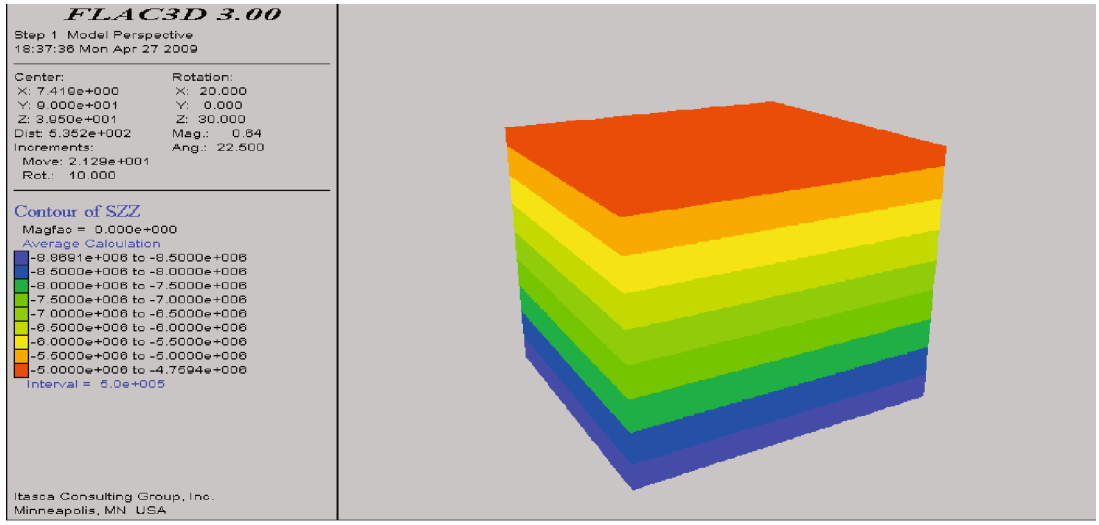

Figure 16: Stress balance vertical stress distribution diagram.

in summary, the bottom plate rupture depth development has not yet reached the test depth of hole 4#.

(4) Analysis of the pore pressure water volume propulsion process of 5# with the cutting eye of working surface (Figure 9)

Because the water pressure of hole 4# is very small, the rock layer rupture depth of bottom plate is determined to be less than the test depth of hole 4#, so the test of hole 5# is finished after -10 m.

4. Base Plate Failure Simulation Calculation

4.1. FLAC3D Boundary Condition Determination. In this simulation, the simulated mining direction is designed to be 200 m in total, the working face width is 180 m, the working face roof is 120 m, the rest of the overlying strata are applied according to the load, and the working face floor simulation thickness is about 40 m (Table 4).

It is generally considered that the compressive strength and cohesion of rock mass are only 0.2~0.3 of rock block parameters, or even smaller. But when the coal is mined under the alluvial strata of North China Plain, the stress state is basically the same. The lateral pressure coefficient is usually 1.0~2.5 in plain area and buried area within 500 m. In this numerical simulation, the lateral pressure coefficient is 1.3. Because the faults that affect the regional structure mainly in this region are mainly north-south normal faults, it is inferred that the pressure on the north-south direction is less than that on the east-west direction, so the lateral pressure coefficient on the X direction is 1.1 and on the Y direction is 1.3.

4.2. Simulation Process and Result Analysis

4.2.1. Simulation Process

(1) Building Geological Models (Figure 15). X direction is set to 200 m, 60 units. Y direction is set to 180 m, 50 units (Table 5).

In the model, the bottom interface of vertical X axis, vertical Y axis, and Z is set as displacement boundary, and the top interface is set as stress boundary. The vertical interface and bottom interface are set as scrolling interface.

(2) Stress Balance. In FLAC3D, after establishing geologic model and giving each element parameter, it is necessary to obtain the balance of each node and element, and excavation calculation can only be performed after the geologic model is balanced. The general stress balance mainly observes the vertical stress.

(3) Excavation. In excavation, set excavation distance to 120 m and -60 m~60 m from X direction. Excavate 5 m every day, calculate 150 steps after excavation, and continue excavation.

4.2.2. Analysis of Results

(1) Distribution Rule of Vertical Stress during Excavation (Figure 16). It can be seen from Figure 17 that the redistribution region of vertical stress during the advance of the working face is as follows (from the direction of advance of the working face): (1) stress release region, (2) stress concentration region, and (3) stress reduction region. (1) Stress release zone is due to the roof rock strata after mining; although some will fall, there is a certain pressure, but in this period of time, the stress still remains reduced. (2) Because there is no mining in front of coal seam and the rear has been recovered, the vertical stress concentration at the tunneling head is about 30 m in width. (3) Stress reduction region is due to the formation of stress concentration region in the middle, corresponding to the occurrence of stress reduction region. The broadband area is 50 m. From Figures 18 and 19, it can be seen that the stress in X direction and Y direction decreases in the goaf range and gradually increases for both sides of the goaf.

Although the lateral pressure is large in the mining process, the stress that controls the coal seam rupture is vertical stress.

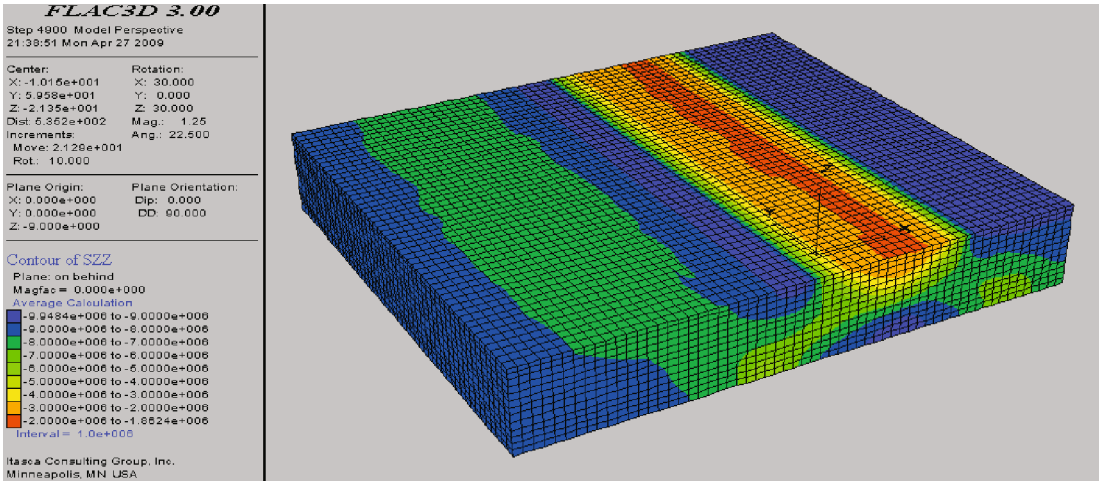

Figure 17: Stress distribution in Z direction of $Z = -9$ plane after excavation.

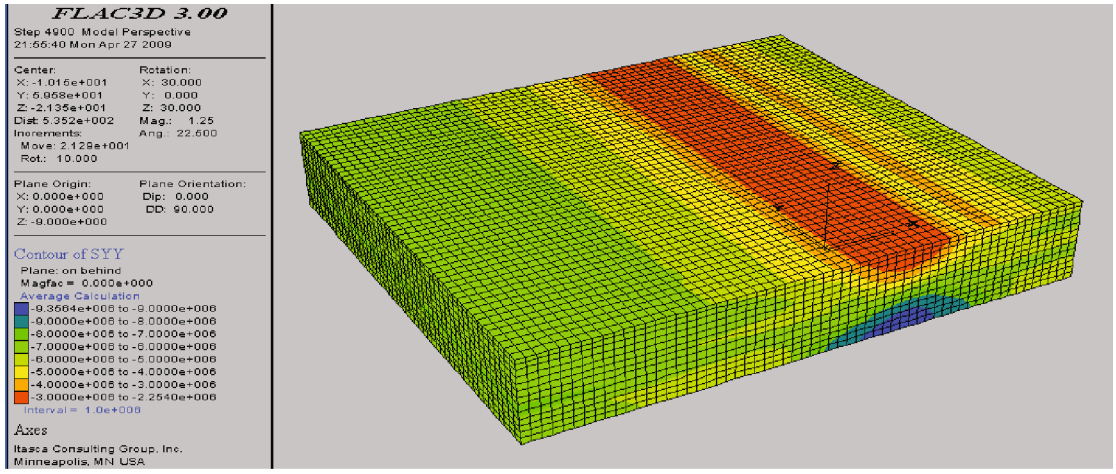

Figure 18: Stress distribution in Y direction of $Z = -9$ plane after excavation.

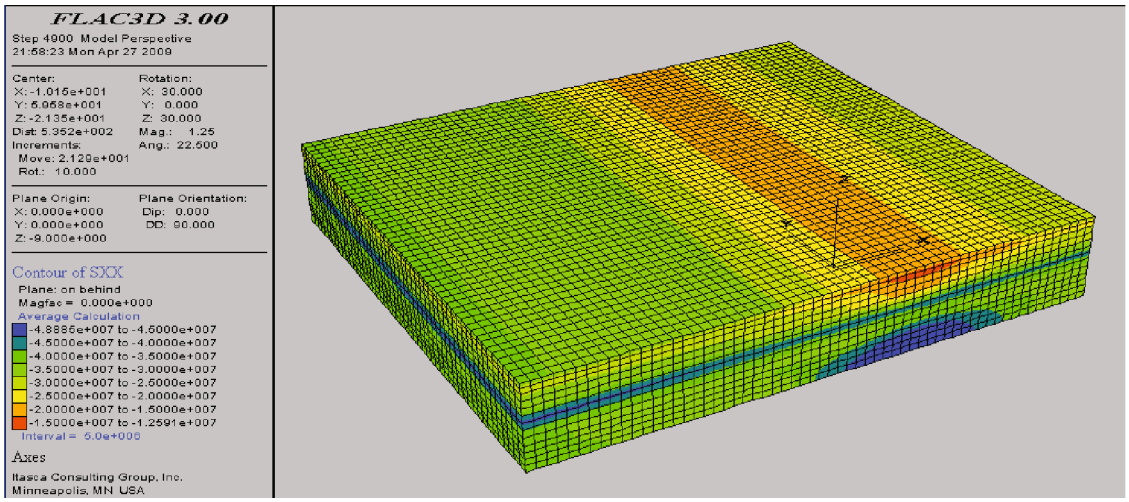

Figure 19: Stress distribution diagram in X direction of $Z = -9$ plane after excavation.

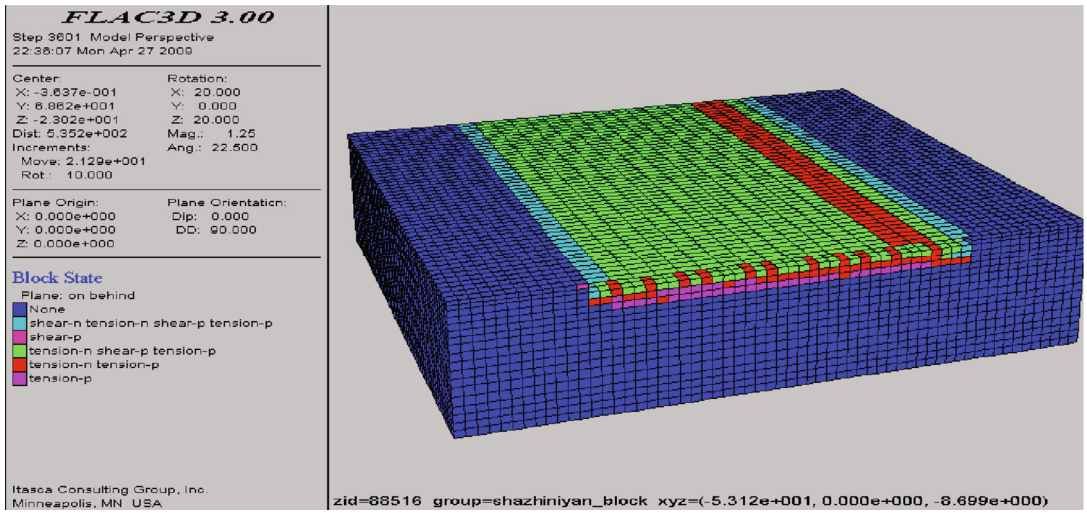

Figure 20: Fracture diagram of coal seam below $Z = 0$ plane after excavation.

(2) Depth of Influence of Coal Seam Mining Floor. From the figure, it can be seen that the rupture and development depth of the floor plate is about 8.7 m (Figure 20).

5. Conclusion

(1) In this bottom plate failure depth test, water injection by embolization method is used to determine the gearing rupture depth. Firstly, single embolic test is used. If the test result is changed greatly from the previous test result, then double embolic test is used to accurately determine the change result, ensuring the accuracy of field test

(2) By two kinds of pressure water tests, the law of floor rupture and development in the process of driving is obtained. That is, when the working face is advanced to the horizontal distance about -50 m from the test point, the water pressure begins to change and gradually decreases. From -40 m to -20, the water pressure begins to recover and basically remains unchanged. When the distance is -20 m, it begins to gradually increase, reaches the maximum from -20 m to 0 m, and then basically remains unchanged. That is, there are three stages in the mining process of the bottom plate failure crack: crack compaction stage, crack compression elastic stage, and crack compression plastic deformation stage

(3) The pressure water test shows that the rupture depth of 10-409 working face occurs at 8.98~9.03 m. The numerical simulation results show that the failure depth of the bottom plate is about 8.7 m. The pressure water test and numerical simulation calculation results are basically the same, which verifies the accuracy of this field pressure water test and also provides a data reference for the evaluation of the water barrier ability of the bottom plate of similar working face and the prevention and control of water by pressure-bearing mining

Data Availability

Some or all data, models, or codes generated or used during the study are available from the corresponding author by request.

Conflicts of Interest

The authors declare that there is no conflict of interest regarding the publication of this paper.

Acknowledgments

The authors acknowledge the support provided by the National Natural Science Foundation of China (51508462).

References

[1] S. Selixalev, *Rock Mechanics and Mine Support*, Fuel Industry Press, Beijing, China, 1954.

[2] Z. Jincai, Z. Yuzhuo, and L. Tianquan, *Rock Seepage and Coal Seam Floor Protrusion*, Geology Press, Beijing, China, 1997.

[3] S. Longqing and H. Jin, "Theory and practice of "four belts" division of coal seam floor," *Journal of China University of Mining and Technology*, vol. 1, pp. 19–26, 2005.

[4] D. Fangjun, L. Zhijun, W. Yarong, Y. Zhirang, Y. Xiping, and Q. Ziwei, "Measures for the treatment of sub-slope well rupture and sand-carrying bottom plate in Yinhe coal mine," *Well-Building Technology*, vol. 42, no. 2, pp. 22–24, 2021.

[5] H. Q. Hao and G. Quan, "Research on damage range of roadway bottom plate and its influence," *Journal of Xi'an University of Science and Technology*, vol. 38, no. 1, pp. 51–58, 2018.

[6] J. Z. Zhangrui and L. Xiuhan, "Other deep coal seam floor mining damage depths," *Journal of Coal Industry*, vol. 38, no. 1, pp. 67–72, 2013.

[7] W. Jiachen, X. Yanchun, X. Gaoming, and J. B. Li, "Application of mine electric profiling method to detect the damage depth of working face bottom plate," *Coal Science and Technology*, vol. 38, no. 1, pp. 97–100, 2010.

[8] L. Haifeng and Y. Duoxi, "A study on the stress distribution law and depth of damage of laminated rocks on shaft plate,"

Journal of Rock Mechanics and Engineering, vol. 33, no. 10, pp. 2030–2039, 2014.

[9] J. Yaodong, L. Yukai, and Z. Yixin, "Similar simulation test on damage regularity of bottom plate of mining face on equal pressure water," *Journal of Rock Mechanics and Engineering*, vol. 30, no. 8, pp. 1571–1578, 2011.

[10] Z. Yixin, J. Yaodong, L. Yukai, and C. Zhijing, "Bidirectional loading similarity simulation test of bottom plate fracture rule of bearing face," *Journal of Coal Industry*, vol. 38, no. 3, pp. 384–390, 2013.

[11] G. Shang, S. Xiaoyu, D. Yanan, L. Pengyang, L. Ming, and L. Heng, "Ground Directional Grouting Technology of Coal Seam Bottom Thin Layer Limestone," *Well Building Technology*, vol. 42, no. 4, pp. 39–44, 2021.

[12] X. Niu, H. Wang, and S. Liu, "Application and development trend of grouting modification Technology for Lower Group Coal Floor Karst Aquifer in Xiuqing Niu, Hua Wang, Shujie Liu North China Coalfield," *Well-Building Technology*, vol. 38, no. 3, pp. 24–30, 2017.

[13] X. Cheng, S. Liu, and D. Liu, "Acoustic CT detection of the damage law of the surrounding rock after coal seam mining," *Journal of Coal Industry*, vol. 26, no. 2, pp. 153–155, 2001.

[14] Z. Pingsong, W. Qian, and L. Shengdong, "Dynamic observation on damage regularity of mining bottom plate," *Journal of Rock Mechanics and Engineering*, vol. 2S, no. S1, pp. 3009–3013, 2006.

[15] Y. B. Hu, W. P. Li, X. M. Chen, H. Xu, and S. Liu, "Temporal and spatial evolution characteristics of fracture distribution of floor strata in deep coal seam mining," *Engineering Failure Analysis*, vol. 132, article 105931, 2022.

[16] K. F. Fan, J. H. He, W. P. Li, and W. Chen, "Dynamic evolution and identification of bed separation in overburden during coal mining," *Rock Mechanics and Rock Engineering*, vol. 55, no. 7, pp. 4015–4030, 2022.

[17] C. Li, J. Zuo, X. Huang, G. Wu, Y. Li, and S. Xing, "Water inrush modes through a thick aquifuge floor in a deep coal mine and appropriate control technology: a case study from Hebei, China," *Mine Water and the Environment*, vol. 41, no. 4, pp. 954–969, 2022.

[18] L. Gang, L. Haizhen, Y. Qinghe, and N. Weifeng, "Failure characteristics of coal seam floor and risk analysis of water inrush in mining with pressure," *China Safety Science Journal*, vol. 32, no. 5, pp. 68–76, 2022.